AIP | Applied Physics Letters

Phase-field modeling of three-phase electrode microstructures in solid oxide fuel cells

Qun Li, Linyun Liang, Kirk Gerdes, and Long-Qing Chen

Citation: Appl. Phys. Lett. **101**, 033909 (2012); doi: 10.1063/1.4738230
View online: http://dx.doi.org/10.1063/1.4738230
View Table of Contents: http://apl.aip.org/resource/1/APPLAB/v101/i3
Published by the American Institute of Physics.

Phase-field modeling of three-phase electrode microstructures in solid oxide fuel cells

Qun Li,[1,2,a)] Linyun Liang,[2] Kirk Gerdes,[3] and Long-Qing Chen[2]
[1]*State Key Laboratory for Mechanical Structural Strength and Vibration, School of Aerospace, Xi'an Jiaotong University, Xi'an 710049, People's Republic of China*
[2]*Department of Materials Science and Engineering, The Pennsylvania State University, University Park, Pennsylvania 16802, USA*
[3]*National Energy Technology Laboratory, Morgantown, West Virginia 26507, USA*

(Received 6 April 2012; accepted 29 June 2012; published online 19 July 2012)

A phase-field model for describing three-phase electrode microstructure (i.e., electrode-phase, electrolyte-phase, and pore-phase) in solid oxide fuel cells is proposed using the diffuse-interface theory. Conserved composition and non-conserved grain orientation order parameters are simultaneously used to describe the coupled phase coarsening and grain growth in the three-phase electrode. The microstructural evolution simulated by the phase-field approach demonstrates the significant dependence of morphological microstructure and output statistic material features on the prescribed kinetic parameters and three-phase volume fractions. The triple-phase boundary fraction is found to have a major degradation in the early evolution. © *2012 American Institute of Physics*. [http://dx.doi.org/10.1063/1.4738230]

Solid oxide fuel cells (SOFC) are anticipated to play a major role in future energy production owing to their potential for clean and efficient electricity generation. The electrode microstructures are known to have a profound effect on the cell performance and durability of SOFC. A typical electrode is a porous mixture of an electron conducting electrode-phase, such as Ni or lanthanum-doped strontium manganate (LSM), and an ion conducting electrolyte phase, such as yttria-stabilized zirconia (YSZ), which facilitates the critical oxygen reduction reaction or fuel oxidation reaction.[1–4] Long-term material degradation induced by microstructural evolution has been considered a primary source of SOFC inefficiency and power losses. Computational modeling efforts have been proposed for multi-scales concern.[5,6] However, most computational works do not examine the microstructure evolution or are limited in either statistical or semi-empirical ways.

On the other hand, the phase-field method has emerged as one of the most powerful methods for modeling transport phenomena and complex microstructural evolution.[7] Furthermore, the phase-field approach can be developed to simulate the microstructure evolution of SOFC functional layers.[8,9] The present paper proposes a general phase-field model for simulating the kinetic of coupled phase coarsening and grain growth in a mesoscale, physics-based three-phase SOFC electrode system. In the phase-field model, two independent composition fields define the volume fractions of the three constituent phases, and two sets of orientation fields are used to represent different crystallographic orientations of electrode-phase and electrolyte-phase. The phase boundaries are described in the spirit of the diffuse-interface theory of Cahn-Hilliard[10] while the grain boundaries are described by the time-dependent Ginzburg-Landau equations.[11] The phase-field approach is numerically developed by semi-implicit spectral method to simulate the microstructural evolution of the SOFC electrode based on the prescribed appropriate kinetic parameters. Computer simulation will allow one to monitor the detailed microstructure evolution and also to obtain the statistical material properties (such as the triple phase boundary (TPB) density) that are critical determinants of cell electrochemical performance.

A porous composite SOFC electrode generally comprises three different phases, i.e., electrode-α-phase (electronic conducting), electrolyte-β-phase (ionic conducting), and pore-γ-phase (gas conducting), as shown in Fig. 1. To describe the phase evolution in such a three-phase system, three composition order parameters $C_\alpha(r)$, $C_\beta(r)$, and $C_\gamma(r)$ are required to represent the corresponding phase volume fractions. The composition field variables are defined as $\{C_\alpha(r), C_\beta(r), C_\gamma(r)\} = \{1, 0, 0\}$ for electrode-α-phase, $\{C_\alpha(r), C_\beta(r), C_\gamma(r)\} = \{0, 1, 0\}$ for electrolyte-β-phase, and $\{C_\alpha(r), C_\beta(r), C_\gamma(r)\} = \{0, 0, 1\}$ for pore-γ-phase. Across the interphase boundary, the composition variables continuously change with finite thickness of the diffuse interfaces. We can eliminate one of the composition order parameters through the constraint condition of volume fractions,

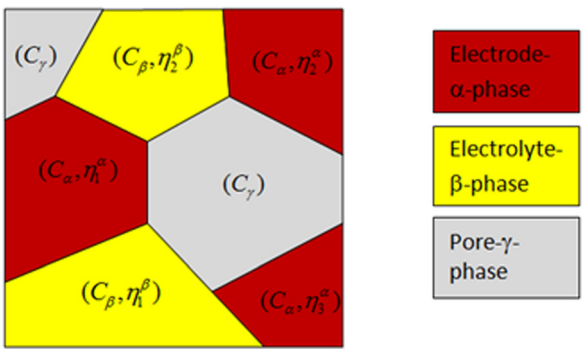

FIG. 1. Schematic description of a three-phase SOFC electrode system (i.e., electrode-α-phase, electrolyte-β-phase, and pore-γ-phase).

[a)]Electronic mail: qunli@mail.xjtu.edu.cn.

i.e., $C_\alpha + C_\beta + C_\gamma = 1$. Therefore, two independent field variables C_α and C_β are sufficient to define the conserved compositions of a three-phase system.

For the fully dense solid electrode-α-phase and electrolyte-β-phase, the grain orientation order parameters are introduced within the diffuse-interface context for representing grains of a given crystallographic orientation in space.

$$\begin{aligned} &C_\alpha(r); \eta_1^\alpha(r), \eta_2^\alpha(r), ..., \eta_p^\alpha(r), \\ &C_\beta(r); \eta_1^\beta(r), \eta_2^\beta(r), ..., \eta_q^\beta(r), \end{aligned} \tag{1}$$

where p and q are the numbers of possible grain orientations of electrode-α-phase and electrolyte-β-phase, respectively. The non-conserved orientation variables change continuously in space and assume continuous values ranging from -1.0 to 1.0. For example, a value of $\eta_i^\alpha(r) = 1.0$ with zero values for all other orientation variables indicates that the material at position r belongs to electrode-α-phase with the crystallographic orientation labeled as i. Note that all orientation field variables are zero for the pore-γ-phase.

The total free energy with the composition and orientation order parameters can be constructed within the diffuse-interface field theory[12,13]

$$F = \int \left[f_0(C_\alpha, C_\beta; \eta_i^\alpha, \eta_i^\beta) + \frac{\kappa_C^\alpha}{2}(\nabla C_\alpha)^2 + \frac{\kappa_C^\beta}{2}(\nabla C_\beta)^2 + \sum_{i=1}^{p} \frac{\kappa_i^\alpha}{2}(\nabla \eta_i^\alpha)^2 + \sum_{i=1}^{q} \frac{\kappa_i^\beta}{2}(\nabla \eta_i^\beta)^2 \right] d^3r, \tag{2}$$

where ∇C_α, ∇C_β, $\nabla \eta_i^\alpha$, and $\nabla \eta_i^\beta$ are gradients of concentration and orientation fields; κ_C^α, κ_C^β and κ_i^α, κ_i^β are the corresponding gradient energy coefficients; f_0 is the local free energy density which is given by

$$f_0 = f_1(C_\alpha) + f_1(C_\beta) + \sum_{i=1}^{p} f_2(C_\alpha, \eta_i^\alpha) + \sum_{i=1}^{q} f_2(C_\beta, \eta_i^\beta) + \sum_{i=1}^{p}\sum_{j\neq i}^{p} f_3(\eta_i^\alpha, \eta_j^\alpha) + \sum_{i=1}^{q}\sum_{j\neq i}^{q} f_3(\eta_i^\beta, \eta_j^\beta) + f_4(C_\alpha, C_\beta), \tag{3}$$

where

$$\begin{aligned} f_1(C) &= -(A/2)(C - C_m)^2 + (B/4)(C - C_m)^4 + (D_\alpha/4)(C - C_0)^4; \\ f_2(C, \eta_i) &= -(\gamma/2)(C - C_0)^2(\eta_i)^2 + (\delta/4)(\eta_i)^4; \\ f_3(\eta_i, \eta_j) &= (\varepsilon_{ij}/2)(\eta_i)^2(\eta_j)^2; \quad f_4(C_\alpha, C_\beta) = (\lambda/2)(C_\alpha)^2(C_\beta)^2, \end{aligned} \tag{4}$$

where $f_1(C)$ is only dependent on the composition variable; $f_2(C, \eta_i)^i$ is the function for coupled composition and orientation fields; $f_3(\eta_i, \eta_j)$ gives the interaction between orientation fields; and $f_4(C_\alpha, C_\beta)$ denotes the coupling between composition fields. The phenomenological parameters in Eq. (4) are assumed as $C_0 = 0.0$, $C_m = 0.5$, $A = 1.0$, $\varepsilon_{ij} = 3.0$, $\delta = 1.0$, $\lambda = 3.0$, $\gamma = \delta$, $B = 4A$, and $D_\alpha = \gamma^2/\delta$. They are chosen in such a way that f_0 has degenerate minima with equal depth located at equilibrium states $C_\alpha(r) = 1, \eta_i^\alpha = 1$ for ith grain of electrode-α-phase; $C_\beta(r) = 1, \eta_j^\beta = 1$ for jth grain of electrolyte-β-phase; $C_\gamma(r) = 1$ for pore-γ-phase. This requirement ensures that each point in space can only belong to a grain with a given orientation of a given phase.

The spatial/temporal kinetics evolution of grain growth and phase coarsening can be described by the time-dependent Ginzburg-Landau equations and Cahn-Hilliard equations

$$\begin{aligned} \frac{\partial \eta_i^\alpha(\mathbf{r}, t)}{\partial t} &= -L_i^\alpha \nabla \left[\frac{\delta f_0}{\delta \eta_i^\alpha(\mathbf{r}, t)} - \kappa_i^\alpha \nabla^2 \eta_i^\alpha \right]; \quad i = 1, 2, ..., p \\ \frac{\partial \eta_i^\beta(\mathbf{r}, t)}{\partial t} &= -L_i^\beta \nabla \left[\frac{\delta f_0}{\delta \eta_i^\beta(\mathbf{r}, t)} - \kappa_i^\beta \nabla^2 \eta_i^\beta \right]; \quad i = 1, 2, ..., q \\ \frac{\partial C_\alpha(\mathbf{r}, t)}{\partial t} &= \nabla \left(M_C^\alpha \nabla \left[\frac{\partial f_0}{\partial C_\alpha(\mathbf{r}, t)} - \kappa_C^\alpha \nabla^2 C_\alpha \right] \right); \\ \frac{\partial C_\beta(\mathbf{r}, t)}{\partial t} &= \nabla \left(M_C^\beta \nabla \left[\frac{\partial f_0}{\partial C_\beta(\mathbf{r}, t)} - \kappa_C^\beta \nabla^2 C_\beta \right] \right); \end{aligned} \tag{5}$$

where L_i and M_C are kinetic coefficients related to grain boundary mobilities and atomic diffusion coefficient, and t is time. The difference between kinetic equations for orientation fields and composition fields comes from the fact that composition is a conserved field which satisfies local and global conservation of phase-volume fractions in a system, whereas the volume fraction of grains of a given orientation is not conserved.

It should be emphasized that the driving force for microstructure evolution is the total interfacial boundary energy. Therefore, the gradient energy coefficients together with the kinetic mobilities are the most important factors to control the kinetics of microstructure evolution. The contact angles at triple junctions obtained by two-dimension simulations are shown in Fig. 2 for the prescribed three sets of gradient energy coefficients. It is found that the equilibrium contact angles at triple junctions are well examined and the gradient coefficients play a key role in determining the contact angles as well as microstructure features of the three-phase system.

Unfortunately, it is very difficult to obtain the actual gradient coefficients and the kinetic mobilities for the SOFC electrode materials. In order to perform the phase-field

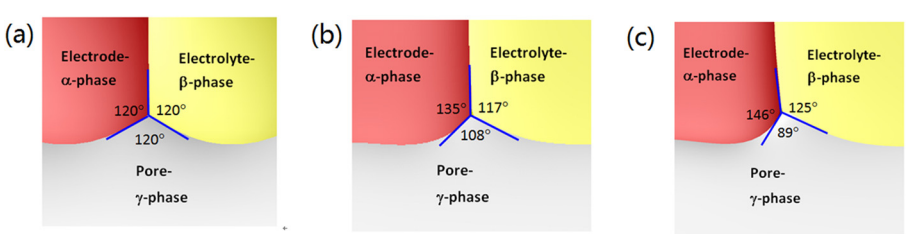

FIG. 2. Equilibrium contact angles at triple junctions for three sets of gradient energy coefficients. (a) $\kappa_C^\alpha = 2.5$ and $\kappa_C^\beta = 2.5$; (b) $\kappa_C^\alpha = 1.5$ and $\kappa_C^\beta = 3.5$; and (c) $\kappa_C^\alpha = 0.5$ and $\kappa_C^\beta = 5.5$.

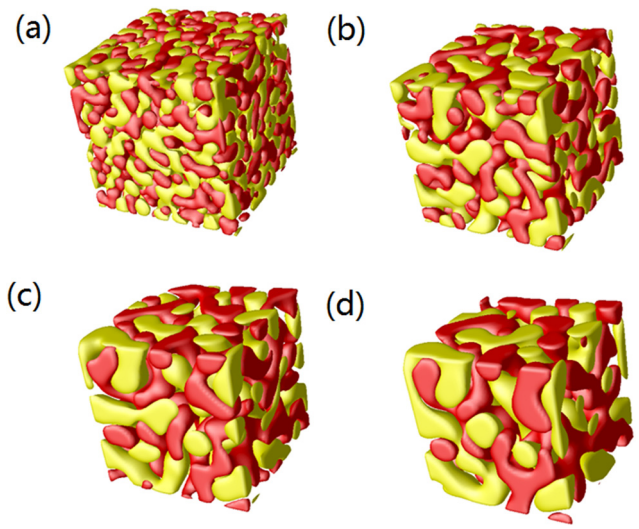

FIG. 3. Temporal microstructural evolution in a three-phase SOFC electrode system. (a) Time step = 1000; (b) time step = 5000; (c) time step = 10 000; and (d) time step = 20 000; The electrode-α-phase, electrolyte-β-phase, and pore-γ-phase are represented in red, yellow, and transparent (with volume fraction 30%, 30%, and 40%, respectively).

model to simulate the specific SOFC electrode microstructure, the gradient energy coefficients as well as other kinetic parameters must be asymptotically evaluated by fitting the experimentally determined interfacial energies ratios or contact angels at feasibly measurable triple junctions. By incorporating the obtained kinetic information into the present diffuse-interface phase-field model, the microstructural evolution of three-phase SOFC electrode can be entirely characterized.

The semi-implicit Fourier-spectral approximation[14,15] can be applied to solve Eq. (5) by transforming the partial differential equations into a sequence of ordinary differential equations in the Fourier space. The semi-implicit Fourier spectral method has capability to provide significantly more accurate results with fewer grid points and greater time step size. A model size of $64\Delta x \times 64\Delta y \times 64\Delta z$ is used and periodic boundary conditions are applied along three directions. The gradient coefficients for phase parameters are $\kappa_i^{\alpha} = 2.5$ and $\kappa_i^{\beta} = 2.5$ and for volume fraction variables are $\kappa_C^{\alpha} = 2.5$ and $\kappa_C^{\beta} = 2.5$. The time step for the evolution is $t = 0.05$ and the spacing $dx = dy = dz = 2.0$. The kinetic coefficients for time-dependent Ginzburg-Landau equations are $L_i^{\alpha} = 2.5$ and $L_i^{\beta} = 2.5$, and the mobilities for Cahn-Hilliard equation are $M_C^{\alpha} = 2.5$ and $M_C^{\beta} = 2.5$.

The temporal three dimensional microstructural evolutions are shown in Fig. 3 where the phase volume fractions are prescribed as: electrode-α-phase: 30%; electrolyte-β-phase: 30%; and pore-γ-phase: 40%. 3D simulations commence from a randomly disordered microstructure where the desired volume fraction and the volume conservation are prescribed. It can be seen from Fig. 3 that the phase coalescence can be trapped and controlled by the inter-particle diffusion through microstructure while the microstructural evolution appears to slow down within a long range. The simulated microstructures possess a striking resemblance to those observed experimentally.[3,4]

The interpenetrating network of electrode-α-phase, electrolyte-β-phase, and pore-γ-phase can also be obtained and shown in Figs. 4(a)–4(c), respectively. The connectivity of each phase is well demonstrated by the phase-field simulation indicating that the volume phases appear to be percolated and are, therefore, electrochemically active. The simulated percolated feature meets the requirement of SOFC electrode microstructure to allow the electronic, ionic, and gas to transport through the electrode (e.g., gas through pore-phase, oxygen ions through electrolyte-phase, and electrons through electrode-phase). Furthermore, the typical simulated microstructures with different volume fractions of each phase are shown in Fig. 5, which demonstrates that the microstructure topology possesses significant dependence on the relative volume fractions of the three phases. All results show that the main features of phase coarsening and various statistical microstructure information are well predicted through the computer simulation by the present phase-field model.

Temporal degradation of TPB segments distributed in a three-phase SOFC electrode system is plotted in Fig. 6. TPB segments are positively assigned if any four neighboring phases contain all three phases with different phases in two diagonal locations. Fig. 6 shows that TPB segments clearly degrade during the temporal evolution. The parametric effect of three sets of gradient coefficients on TPB fractions is performed and plotted in Fig. 7 with the fixed three phase volume fractions. In Fig. 7, different prescribed gradient coefficients lead to similar trends of TPB degradation behavior. Rapid degradation occurs within the early evolutionary

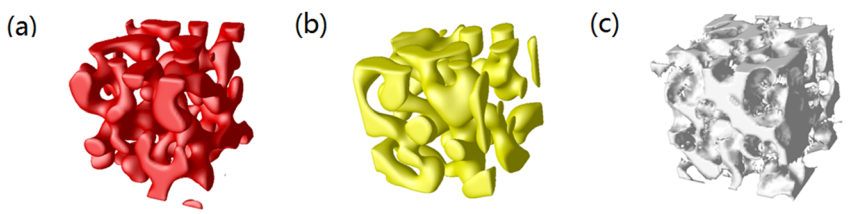

FIG. 4. Percolation phase network in SOFC electrode. (a) electrode-α-phase; (b) electrolyte-β-phase; and (c) pore-γ-phase.

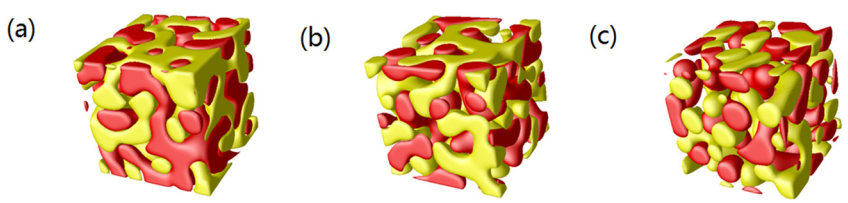

FIG. 5. Microstructure of three-phase SOFC electrode for different volume fractions of electrode-α-phase/electrolyte-β-phase/pore-γ-phase: (a) 35%-35%-30%; (b) 30%-30%-40%; and (c) 25%-25%-50%.

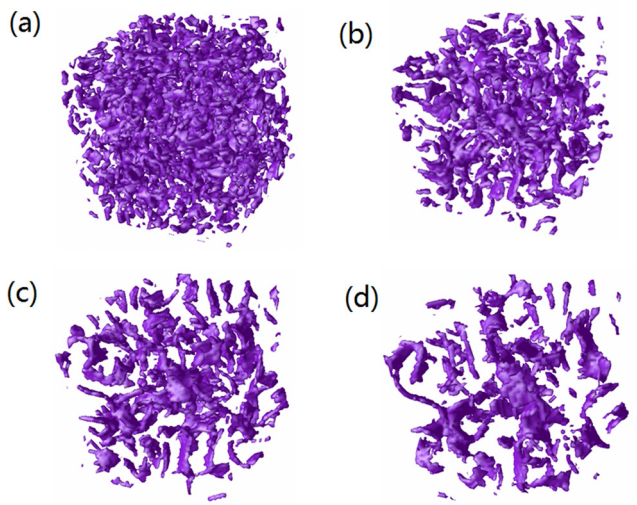

FIG. 6. Temporal degradation of TPB segments distributed in a three-phase SOFC electrode system. (a) Time step = 1000; (b) time step = 5000; (c) time step = 10 000; and (d) time step = 20 000; The electrode-α-phase, electrolyte-β-phase, and pore-γ-phase are with volume fractions of 30%, 30%, and 40%, and $\kappa_C^{\alpha} = 1.5$ and $\kappa_C^{\beta} = 3.5$ are prescribed in phase-field numerical simulations.

period, though degradation in the TPB fraction slows over longer time periods. Actually, the temporal degradation of TPB is qualitatively consistent with the temporal phase coarsening evolution of microstructure, which indicates that particle agglomeration and coarsening may be principal factors responsible for electrode degradation. It should be pointed that a random disordered microstructure was used as the initial input for the phase-field model. This randomization can lead to a slightly different TPB number and two-solid phase contact number. However, the tendency of evolution of TPB number and two-solid phase contact number is similar even for different randomization.

Fig. 8 shows the temporal evolution of TPB fraction for different three-phase volume fractions in SOFC electrode. The general trend of electrode degradation remains similar regardless of the phase volume fractions. At the early evolution time, there is a rapid decrease of the TPB. Thereafter, the TPB fractions almost stabilize with the negligible reduction, which is consistent with the stabilization of morphological microstructure after the long time operation. However, the magnitude of TPB fraction shows a significant dependence on the three-phase volume fraction. The guidelines of the dependence of TPB behaviors on phase volume fractions as well as gradient coefficients can be potentially established by the phase-field computation simulation. There is a potential opportunity for improving the long-time performance of SOFC electrode by controlling the phase volume fractions or the surface/interfacial energies in materials. The model may also inform design of the optimized TPB or means to mitigate TPB degradation.

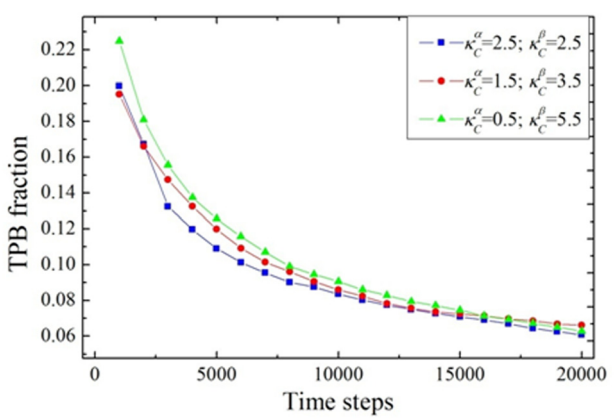

FIG. 7. Temporal evolution of TPB fraction for three sets of gradient coefficients with the fixed volume fraction of electrode-α-phase: 30%, electrolyte-β-phase: 30%, and pore-γ-phase: 40%.

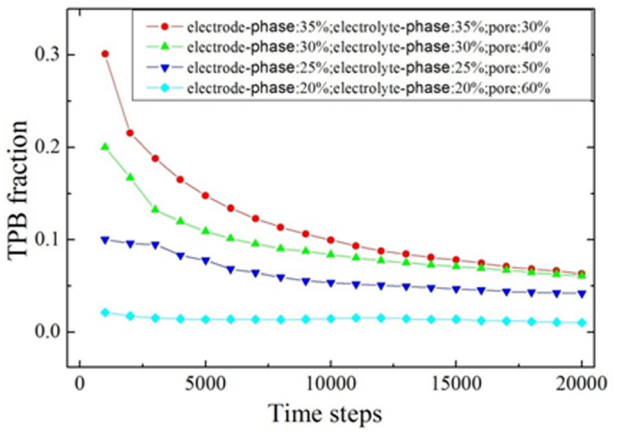

FIG. 8. Temporal evolution of TPB fraction for different three-phase volume fractions with the fixed gradient coefficient $\kappa_C^{\alpha} = 1.5$ and $\kappa_C^{\beta} = 3.5$.

It is evident that the phase-field model can efficiently support evaluations of fundamental performance parameters and long-range microstructural evolution. Nevertheless, it should be noted that the calculation accuracy of overall statistical material properties as well as the morphological evolution with time scale during the long-range of operation can be further improved by calibrating factors associated with the phase-field simulations. These factors include the actual initial microstructure and the accurate values of mobilities, diffusivities, and interfacial energies ratios or contact angles *etc.,* which can be asymptotically evaluated or available from the corresponding experimental measure. With inclusion of appropriate kinetic and dynamic parameters, the present phase-field model is tunable to allow more accurate simulation of the specific SOFC electrode microstructure, e.g., LSM-YSZ-cathode, LSCF-SDC($La_{0.58}Sr_{0.4}Co_{0.2}Fe_{0.8}O_{3-\delta}$–$Ce_{0.8}Sm_{0.2}O_{2-\delta}$)-cathode, Ni-YSZ-anode, or Ni-SDC-anode, etc.

In summary, a computer simulation approach based on the phase-field model is developed for investigating microstructure evolution in three-phase SOFC electrode system. The proposed simulation framework reproduces the electrode microstructure features for the prescribed kinetic parameters and three-phase volume fractions. The phase-field model can be used to predict the morphology of three-phase cathode and anode microstructure. The useful statistical material features and the effect of evolving microstructures on the statistical material properties such as TPB are obtained. Continued maturation of this approach will result in robust computationally guided material design that accelerates microstructure and materials optimization of novel SOFC electrodes and supports evaluation of long-term cell degradation.

This technical effort was performed in support of the National Energy Technology Laboratory's on-going research in the area of cathode modeling in Solid Oxide Fuel Cells under the RDS Contract 10-220621 6923. Fruitful discussions of basic ideas contained in this paper were conducted with Professor Paul Salvador and Dr. Sudip Bhattacharya. The author Qun Li also thanks the support by the National Natural Science Foundation of China with Grant Nos. 10932007 and 11021202 and the Fundamental Research Funds for the Central Universities in China.

[1]W. Z. Zhu and S. C. Deevi, Mater. Sci. Eng. A **362**, 228 (2003).
[2]J. R. Wilson, W. Kobsiriphat, R. Mendoza, H. Y. Chen, J. M. Hiller, D. J. Miller, K. Thornton, P. W. Voorhees, S. B. Adler, and S. A. Barnett, Nature Mater. **5**, 541 (2006).
[3]J. R. Wilson, A. T. Duong, M. Gameiro, H. Y. Chen, K. Thornton, D. R. Mumm, and S. A. Barnett, Electrochem. Commun. **11**, 1052 (2009).
[4]N. Shikazono, D. Kanno, K. Matsuzaki, H. Teshima, S. Sumino, and N. Kasagi, J. Electrochem. Soc. **157**, B665 (2010).
[5]S. Kakaç, A. Pramuanjaroenkij, and X. Y. Zhou, Int. J. Hydrogen Energy **32**, 761 (2007).
[6]V. M. Janardhanan and O. Deutschmann, Phys. Chem. **221**, 443 (2007).
[7]L. Q. Chen, Ann. Rev. Mater. Res. **32**, 113 (2002).
[8]J. H. Kim, W. K. Liu, and C. Lee, Comput Mech. **44**, 683 (2009).
[9]H. Y. Chen, H. C. Yu, J. S. Cronin, J. R. Wilson, S. A. Barnett, and K. Thornton, J. Power Sources **196**, 1333 (2011).
[10]J. W. Cahn, Acta Metall. **9**, 795 (1961).
[11]J. W. Cahn and S. M. Allen, J. Phys. **38**, C7 (1977).
[12]L. Q. Chen and D. N. Fan, J. Am. Ceram. Soc. **79**, 1163 (1996).
[13]D. N. Fan, S. P. Chen, L. Q. Chen, and P. W. Voorhees, Acta Mater. **50**, 1895 (2002).
[14]L. Q. Chen and J. Shen, Comput. Phys. Commun. **108**, 147 (1998).
[15]J. Z. Zhu, L. Q. Chen, J. Shen, and V. Tikare, Phys. Rev. E **60**, 3564 (1999).